Inorganic Chemistry

pubs.acs.org/IC

Article

Effect of Lewis Acids on the Structure and Reactivity of a Mononuclear Hydroxomanganese(III) Complex

Derek B. Rice, Elizabeth N. Grotemeyer, Anna M. Donovan, and Timothy A. Jackson*

Cite This: *Inorg. Chem.* 2020, 59, 2689−2700

Read Online

ACCESS | Metrics & More | Article Recommendations | Supporting Information

ABSTRACT: The addition of $Sc(OTf)_3$ and $Al(OTf)_3$ to the mononuclear Mn^{III}-hydroxo complex $[Mn^{III}(OH)(dpaq)]^+$ (**1**) gives rise to new intermediates with spectroscopic properties and chemical reactivity distinct from those of $[Mn^{III}(OH)(dpaq)]^+$. The electronic absorption spectra of $[Mn^{III}(OH)(dpaq)]^+$ in the presence of $Sc(OTf)_3$ (**1**-Sc^{III}) and $Al(OTf)_3$ (**1**-Al^{III}) show modest perturbations in electronic transition energies, consistent with moderate changes in the Mn^{III} geometry. A comparison of ^{1}H NMR data for **1** and **1**-Sc^{III} confirm this conclusion, as the ^{1}H NMR spectrum of **1**-Sc^{III} shows the same number of hyperfine-shifted peaks as the ^{1}H NMR spectrum of **1**. These ^{1}H NMR spectra, and that of **1**-Al^{III}, share a similar chemical-shift pattern, providing firm evidence that these Lewis acids do not cause gross distortions to the structure of **1**. Mn K-edge X-ray absorption data for **1**-Sc^{III} provide evidence of elongation of the axial Mn−OH and Mn−N(amide) bonds relative to those of **1**. In contrast to these modest spectroscopic perturbations, **1**-Sc^{III} and **1**-Al^{III} show greatly enhanced reactivity toward hydrocarbons. While **1** is unreactive toward 9,10-dihydroanthracene (DHA), **1**-Sc^{III} and **1**-Al^{III} react rapidly with DHA (k_2 = 0.16(1) and 0.25(2) M^{-1} s^{-1} at 50 °C, respectively). The **1**-Sc^{III} species is capable of attacking the much stronger C−H bond of ethylbenzene. The basis for these perturbations to the spectroscopic properties and reactivity of **1** in the presence of these Lewis acids was elucidated by comparing properties of **1**-Sc^{III} and **1**-Al^{III} with the recently reported Mn^{III}−aqua complex $[Mn^{III}(OH_2)(dpaq)]^{2+}$ (*J. Am. Chem. Soc.* **2018**, *140*, 12695−12699). Because **1**-Sc^{III} and **1**-Al^{III} show ^{1}H NMR spectra essentially identical to that of $[Mn^{III}(OH_2)(dpaq)]^{2+}$, the primary effect of these Lewis acids on **1** is protonation of the hydroxo ligand caused by an increase in the Brønsted acidity of the solution.

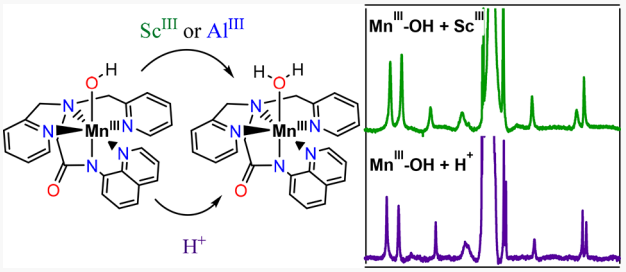

INTRODUCTION

Mononuclear manganese−hydroxo adducts have been proposed to be vital intermediates in manganese-dependent enzymes such as manganese lipoxygenase (MnLOX).[1−4] In this enzyme, a Mn^{III}−hydroxo adduct is proposed to abstract a hydrogen atom from a polyunsaturated fatty acid substrate to initiate its dioxygenation. One means of further understanding the basis for this biological reaction comes through the use of model complexes.[5] With such complexes, the effects of small perturbations to the ligand environment can be correlated with changes in structure and reactivity.

A current challenge with Mn^{III}−hydroxo model complexes lies in the paucity of complexes able to oxidize C−H bonds with bond dissociation energies similar to that of the MnLOX substrate. The only Mn^{III}−hydroxo complexes that have been reported to perform C−H bond activation are the $[Mn^{III}(OH)(PY5)]^{2+}$ complex, from Stack et al.,[6] and the $[Mn^{III}(OH)(dpaq)]^+$ and $[Mn^{III}(OH)(dapq^{2Me})]^+$ complexes from our group (PY5 = 2,6-bis(bis(2-pyridyl)-methoxymethane)pyridine; dpaq = 2-(bis(pyridine-2-ylmethyl))amino-*N*-quinolin-8-ylacetamidate; $dpaq^{2Me}$ = 2-(bis(pyridine-2-ylmethyl))amino-*N*-2-methylquinolin-8-ylacetamidate).[7,8] The $[Mn^{III}(OH)(PY5)]^{2+}$ complex, which features a neutral, pentadentate ligand, is capable of reacting with substrates such as toluene (C−H bond dissociation free energy, BDFE, of 88 kcal mol^{-1}) with a second-order rate constant (k_{2corr}, which has been corrected for the number of C−H bonds of equivalent strength) of 2.2 × 10^{-3} M^{-1} s^{-1} at 50 °C.[6] In contrast, $[Mn^{III}(OH)(dpaq)]^+$ and $[Mn^{III}(OH)(dpaq^{2Me})]^+$, which contain monoanionic, pentadentate ligands with an amide function trans to the hydroxo ligand (Figure 1), are only capable of attacking the weak C−H bond of xanthene (BDFE = 75 kcal mol^{-1}), with a pseudo-first-order rate constant of ca. 8 × 10^{-4} s^{-1} (k_{obs}, at 250 equiv of xanthene) at 50 °C.[7,8] Mononuclear Mn^{III}−oxo complexes, with strong hydrogen-bonding interactions with adjacent ureayl H−N moieties, have also been reported to oxidize activated C−H bonds.[9]

To understand how ligand perturbations tune the reactivity of Mn^{III}−hydroxo units, we recently synthesized a series of derivatives of $[Mn^{III}(OH)(dpaq)]^+$, where the 5-position of the quinoline was substituted with electron-donating and

Received: October 9, 2019
Published: February 11, 2020

https://dx.doi.org/10.1021/acs.inorgchem.9b02980
Inorg. Chem. 2020, 59, 2689−2700

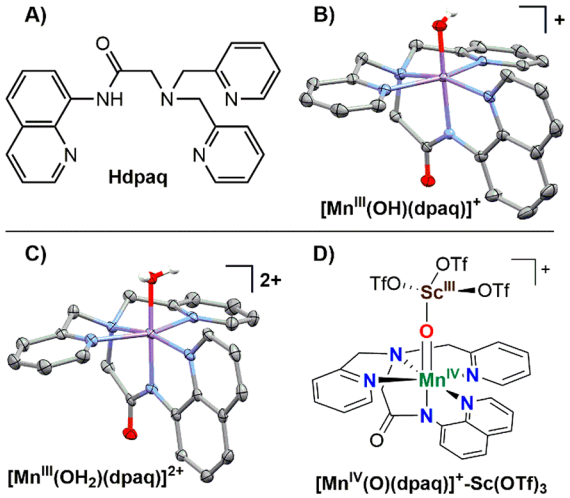

Figure 1. Structure of Hdpaq ligand (A), X-ray diffraction structures of $[Mn^{III}(OH)(dpaq)]^+$ (B)[8] and $[Mn^{III}(OH_2)(dpaq)]^{2+}$ (C),[10] and proposed structure of the Sc^{III} adduct of $[Mn^{IV}(O)(dpaq)]^+$ from ref 11.

-withdrawing groups ($[Mn^{III}(OH)(dpaq^{5\text{-}R})]^+$).[12] This position, which is para to the amide nitrogen, provides tuning of the donor properties of the ligand trans to the hydroxo. Among this series, the inclusion of electron-withdrawing substituents (-Cl and $-NO_2$) led to more positive $Mn^{III/II}$ reduction potentials, as expected. However, these changes in potential were correlated with only modest (ca. 8-fold) rate increases for the oxidation of TEMPOH (TEMPOH = 2,2′,6,6′-tetramethylpiperidine-1-ol) among this series of Mn^{III}–hydroxo complexes.[12]

As an alternative means of enhancing oxidative reactivity, Nam and co-workers reported that the reaction of $[Mn^{III}(OH)(dpaq)]^+$ with triflic acid generates the Mn^{III}–aqua species $[Mn^{III}(OH_2)(dpaq)]^{2+}$, which was structurally characterized by X-ray crystallography (Figure 1C).[10] The Mn^{III}–aqua complex showed substantial rate enhancements in O–H bond oxidation relative to the Mn^{III}–hydroxo analogue.[10] Specifically, $[Mn^{III}(OH_2)(dpaq)]^{2+}$ reacted with 2,6-di-*tert*-butyl-4-methoxyphenol ca. 240-fold faster than $[Mn^{III}(OH)(dpaq)]^+$. The enhanced reactivity of the Mn^{III}–aqua adduct was attributed to the substantially higher $Mn^{III/II}$ reduction potential when compared to the Mn^{III}–hydroxo analogue (1.03 and −0.1 V versus SCE, respectively).[10] Recently, Borovik and co-workers have probed the influence of hydrogen bonds on the reactivity of Mn^{III}–oxo complexes by modulating the basicity of an appended hydrogen-bond donor to the oxo ligand.[9]

A complementary method of tuning oxidation reactivity, which has been widely used for high-valent Fe–oxo[13−15] and Mn–oxo complexes,[16−28] is to form Lewis-acid adducts of metal complexes.[29] Of most relevance to the modest reactivity differences for the $[Mn^{III}(OH)(dpaq^{5\text{-}R})]^+$ series, Yang and co-workers have shown that the reactivity of iron and manganese salen complexes is more strongly perturbed by interactions with Lewis acids than by modification of the ligand scaffold using electron-donating and -withdrawing substituents.[30,31] Thus, interactions of $[Mn^{III}(OH)(dpaq)]^+$ with Lewis acids could lead to more dramatic rate enhancements, perhaps on par with those observed for the Mn^{III}–aqua analogue.[10]

Recently, Nam and co-workers have described Lewis-acid adducts of a Mn^{IV}–oxo adduct supported by the dpaq ligand (Figure 1D).[11,32] Addition of Lewis acids of varied strength (from Sc^{III} to Ca^{II}) to $[Mn^{III}(OH)(dpaq)]^+$ followed by iodosobenzene (PhIO) oxidation led to the formation of the putative $[Mn^{IV}(O)(dpaq)]^+$–Lewis-acid complexes. An interaction between the Lewis acid and the oxo ligand of $[Mn^{IV}(O)(dpaq)]^+$ was inferred from analysis of Mn K-edge extended X-ray absorption fine structure (EXAFS) data, and evidence for the Mn^{IV} oxidation state was provided by EPR measurements.[11] Lewis-acid binding was shown to modulate the oxygen-atom, hydrogen-atom, and electron transfer reactivities of the Mn^{IV}–oxo unit. An increase in the strength of the Lewis acid led to enhancements in oxygen-atom and electron transfer rates, while stronger Lewis acids were associated with slow hydrogen-atom transfer rates. While the formulation of these Mn^{IV}–oxo–Lewis-acid adducts has recently been questioned,[33] the results nonetheless show a strong effect of Lewis acids on reactivity, even if the corresponding cause is uncertain.

One significant challenge in the investigations described above is the lack of experimental information regarding the interaction between the Lewis acid and the high-valent Mn–oxo species under conditions directly relevant to the kinetic investigations. In some cases, formation of a Mn═O···LA adduct (where LA represents the Lewis acid) is inferred from analysis of EXAFS data, which often reveal weak metal–metal scattering peaks attributed to the Lewis acids.[18,19] However, these EXAFS data are collected for frozen solutions at temperatures far lower than those employed for the kinetic investigations. In addition, while the weak metal–metal signals could reflect the Mn═O···LA angle, with angles of less than 150° expected to give rise to very weak scattering,[21] it is important to bear in mind past cases where EXAFS signatures attributed to metal–metal scattering were re-evaluated in terms of a collection of carbon scatterers.[34] A means of probing solution-phase interactions of metal–oxygen species with Lewis acids at temperatures relevant to those of kinetic investigations is necessary for better understanding the structures of these systems.

In this work, we evaluate the influence of the Lewis-acid salts $Sc(OTf)_3$ and $Al(OTf)_3$ on the structure and reactivity of the Mn^{III}–hydroxo unit of $[Mn^{III}(OH)(dpaq)]^+$. Importantly, the effects of these Lewis acids on the properties of the Mn^{III}–hydroxo complex can be monitored by room-temperature ^1H NMR and electronic absorption measurements, as employed previously to understand the solution properties of $[Mn^{III}(OH)(dpaq)]^+$ and its derivatives.[12,35] On the basis of these experimental data, the reactions of $Sc(OTf)_3$ and $Al(OTf)_3$ with $[Mn^{III}(OH)(dpaq)]^+$ in MeCN in the presence of added H_2O leads to the formation of new intermediates. These intermediates show oxidative reactivity greatly enhanced relative to that of $[Mn^{III}(OH)(dpaq)]^+$. Remarkably, the spectroscopic and kinetic data for $[Mn^{III}(OH)(dpaq)]^+$ in the presence of either $Sc(OTf)_3$ or $Al(OTf)_3$ are essentially identical to those of the Mn^{III}–aqua complex $[Mn^{III}(OH_2)(dpaq)]^{2+}$. Therefore, we conclude that the primary influence of these Lewis acids is to increase the Brønsted acidity of the solution, promoting protonation of the Mn^{III}–hydroxo unit.

EXPERIMENTAL SECTION

Materials and Instrumentation. All chemicals were obtained from commercial vendors at ACS grade or better and were used without further purification unless otherwise noted. Acetonitrile and diethyl ether were dried and degassed using a PureSolv solvent

https://dx.doi.org/10.1021/acs.inorgchem.9b02980
Inorg. Chem. 2020, 59, 2689−2700

purification system. [Mn^{II}(dpaq)](OTf) and [Mn^{III}(OH)dpaq)](OTf) were prepared as reported previously.[8] 9,10-Dihydroanthracene was purified by recrystallization from ethanol before use. Electronic absorption spectroscopy was performed using an Agilent 8453 spectrophotometer interfaced with a Unisoku cryostat. EPR experiments were performed on a Bruker EMXplus with Oxford ESR900 continuous-flow liquid helium cryostat and Oxford ITC503 temperature system.

Reactions of [Mn^{III}(OH)(dpaq)]$^+$ with $Sc(OTf)_3$, $Al(OTf)_3$, and $HClO_4$. A 1.25 mM solution of [Mn^{III}(OH)(dpaq)](OTf) (**1**) in 2 mL of MeCN was prepared in an argon-filled glovebox, placed in a gastight cuvette, and sealed with a septum. A solution of 2 equiv of $Sc(OTf)_3$ was prepared in 100 μL of MeCN and stored in a gastight syringe. For formation of intermediate **1**-Sc^{III}, a 100 μL aliquot of a 90:10 (v:v) $CH_3CN:H_2O$ stock solution, which had been sparged with N_2 gas, was first added to the cuvette to generate a solution of **1** that is 99:1 (v:v) MeCN:H_2O). Next, a 100 μL aliquot of the $Sc(OTf)_3$ solution was added at 50 °C. The reaction was monitored by electronic absorption spectroscopy. **1**-Al^{III} was prepared similarly using 2 equiv of $Al(OTf)_3$ in 100 μL of MeCN. For formation of the intermediate **1**-H^+, a solution capable of delivering 1 equiv of $HClO_4$ in 100 μL was prepared and added to the cuvette following the addition of 100 μL of 90:10 (v:v) $CH_3CN:H_2O$.

Acquisition of ^{1}H NMR Data. ^{1}H NMR samples of **1**-Sc^{III} or **1**-Al^{III} were prepared by adding 2 equiv of $Sc(OTf)_3$ or $Al(OTf)_3$, respectively, in MeCN-d_3 to 2.5 mM solutions of **1** in 98:2 (v:v) MeCN-d_3:D_2O. The higher water ratio was employed as these ^{1}H NMR experiments are performed with a greater total Mn^{III} concentration than the electronic absorption and kinetic experiments. ^{1}H NMR samples of [$Mn^{III}(OH_2)$(dpaq)]$^{2+}$ (**1**-H^+) were prepared by adding 1 equiv of $HClO_4$ in MeCN-d_3 to 2.5 mM solution of **1** in 98:2 (v:v) MeCN-d_3:D_2O. All ^{1}H NMR data were collected on a 400 MHz Bruker AVIIIHD NMR with an acquisition time of 0.27 s and a D1 of 0 s with a spectral width of 150 to −100 ppm. At least 1000 scans were accumulated to provide sufficient signal-to-noise for each sample. Spectra were baseline-subtracted with the multipoint fitting procedure using spline functions as available in MestReNova.

XAS Experiments for 1-Sc^{III}. A frozen solution sample of **1**-Sc^{III} was generated by preparing a 2.5 mM solution of **1** in 2 mL of MeCN and adding 20 μL of H_2O and 2 equiv of $Sc(OTf)_3$. Once **1**-Sc^{III} was maximally formed, as judged by electronic absorption spectroscopy, an aliquot of the solution was transferred to an XAS sample cup and rapidly frozen in liquid nitrogen. Mn K-edge XAS data were obtained via fluorescence excitation at beamline 9-3 at Stanford Synchrotron Radiation Lightsource (SSRL) at 7 K using a Si(220) monochromator and a 100-element Ge array detector. Data were collected over an energy range of 6400−7250 eV. A manganese foil was used as a reference, and internal calibration was performed by assigning the edge energy of the foil to 6539.0 eV. EXAFS data analysis was performed using the *DEMETER* software package, and fitting was carried out in *ARTEMIS* on the $k_3\chi(k)$ data.[36] *FEFF6*[37] was used to generate the phase and amplitude functions from the crystal structure of [Mn^{III}(OH)(dpaq)](OTf).[8] For the fits, the parameters R (average scattering pathway distance) and σ^2 (Debye−Waller factor) were optimized individually, and the E_0 parameter was a common variable for all paths. The n (degeneracy) parameter was fixed for each fit and varied between fits.

Kinetic Investigations of the Reactivity of 1-Sc^{III}, 1-Al^{III}, and 1-H^+ with Hydrocarbons. The determination of second-order rate constants for the oxidation of DHA by **1**-Sc^{III}, **1**-Al^{III}, and **1**-H^+ and oxidation of ethylbenzene by **1**-Sc^{III} was performed using essentially identical experimental procedures. Here we describe the procedure employed for **1**-Sc^{III} as a representative example; experiments for **1**-Al^{III} and **1**-H^+ were performed in the same manner, with the use of $Al(OTf)_3$ and $HClO_4$, respectively, rather than $Sc(OTf)_3$. A 1.25 mM solution of **1**-Sc^{III} was generated as described above, with the exception that the solution was first heated to 50 °C in a Unisoku cryostat interfaced with an Agilent 8453 spectrophotometer. The $Sc(OTf)_3$ solution was then added to the cuvette (to give 2 equiv of Sc^{III} relative to **1**), and **1**-Sc^{III} was allowed to form maximally, as determined by following the absorbance at 700 nm. At maximal formation of **1**-Sc^{III}, an aliquot of a CH_2Cl_2 solution containing excess substrate (DHA or ethylbenzene; typically in a concentration range to give 10−200 equiv relative to **1**-Sc^{III}) was added. The ensuing reaction was monitored by disappearance of the signal at 700 nm. Pseudo-first-order rate constants (k_{obs}) determined at different equivalents of substrate were used to determine a second-order rate constant by fitting a plot of k_{obs} versus substrate concentration to a linear function. To identify organic products, the reaction mixture was passed through a silica plug. The organic products were eluted with CH_2Cl_2. The eluent was dried, and 1 equiv of benzoquinone (relative to the total manganese concentration) benzoquinone was added as an internal standard. The solids were dissolved in $CDCl_3$, and the reaction products were analyzed by ^{1}H NMR spectroscopy.

IR Data Collection. Solution-phase IR samples of **1**-Sc^{III} were prepared by adding 2 equiv of $Sc(OTf)_3$ to a 12.5 mM solution of **1** in 97:3 (v:v) MeCN:H_2O. Solution-phase IR spectra were collected on a ReactIR iC10 with a K4 conduit and SiComp probe. For reference, spectra were also collected for a 12.5 mM solution of **1** in 97:3 MeCN:H_2O, a 97:3 MeCN:H_2O solution, and a 97:3 MeCN:H_2O solution with 25 mM $Sc(OTf)_3$. Solid-state FT-IR data were collected for **1** and **1**-Sc^{III}. The latter was prepared by adding 2 equiv of $Sc(OTf)_3$ to 2.5 mM solutions of **1** in 98:2 (v:v) MeCN:H_2O. The resulting solution was then added dropwise to cold ether, which resulted in the precipitation of a green powder. All solid-state FT-IR data were collected on a PerkinElmer Spectrum 100 FT-IR spectrometer with samples prepared as KBr pellets.

RESULTS AND DISCUSSION

Formation of Intermediates 1-Sc^{III} and 1-Al^{III} by Reaction of [Mn^{III}(OH)(dpaq)]$^+$ with $Sc(OTf)_3$ and $Al(OTf)_3$, Respectively. We have previously reported that when [Mn^{III}(OH)(dpaq)](OTf) (**1**) is dissolved in dried MeCN, the Mn^{III}−hydroxo adduct establishes an equilibrium with the dinuclear [$Mn^{III}Mn^{III}$(μ-O)$(dpaq)_2$]$^{2+}$ complex (Scheme 1).[35]

Scheme 1. Equilibrium between Mononuclear Hydroxomanganese(III) and Dinuclear (μ-Oxo)dimanganese(III,III) Complexes

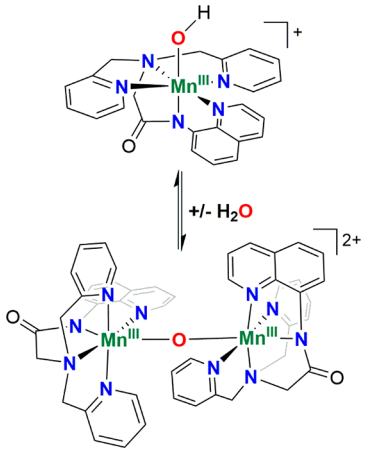

The addition of a small amount of H_2O (880 equiv relative to the total Mn; i.e., a 99:1 (v:v) MeCN:H_2O solution for a 2 mM solution of **1**) results in a shift of the equilibrium such that the Mn^{III}−hydroxo species becomes dominant in solution. When Lewis acids are added to **1** in dried MeCN, any ensuing reaction would be complicated by the presence of both [Mn^{III}(OH)(dpaq)]$^+$ and [$Mn^{III}Mn^{III}$(μ-O)$(dpaq)_2$]$^{2+}$ in solution, whereas this complication should be minimized when Lewis acids are added to **1** in MeCN:H_2O mixtures. The

https://dx.doi.org/10.1021/acs.inorgchem.9b02980
Inorg. Chem. 2020, 59, 2689−2700

recent reports of $[Mn^{IV}(O)(dpaq)]^+$ and $[Mn^{IV}(O)(dpaq)]^+$–Lewis-acid complexes did not note the addition of water to the MeCN solutions prior to oxidation by PhIO.[11,33]

When 2 equiv of $Sc(OTf)_3$ is added to **1** dissolved in a 99:1 (v:v) MeCN:H_2O solution at 25 °C, we observe the formation of electronic absorption bands at 350, 410, 510 (shoulder), 700, and 1150 nm (Figure 2 and Table 1; the near-IR

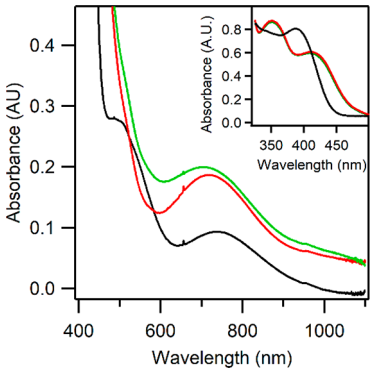

Figure 2. Electronic absorption spectra of 2 mM $[Mn^{III}(OH)(dpaq)](OTf)$ (**1**) in 2 mL of 99:1 (v:v) MeCN:H_2O before (black trace) and after the addition of 2 equiv of $Sc(OTf)_3$ (**1**-Sc^{III}; green trace) or 2 equiv of $Al(OTf)_3$ (**1**-Al^{III}; red trace) at 25 °C. The inset shows the UV region for reactions that are 0.25 mM in **1**.

absorption feature is evident in Supporting Information Figure S1). The new intermediate formed under these conditions will be referred to as **1**-Sc^{III}, simply to signify that this intermediate is formed by the reaction of **1** with $Sc^{III}(OTf)_3$. The naming scheme does not necessarily reflect any direct interaction between $Sc^{III}(OTf)_3$ and **1**. The electronic absorption features observed for **1**-Sc^{III} are very similar to those reported for the $[Mn^{IV}(O)(dpaq)]^+$–Lewis-acid adducts, when the Lewis acids are Sc^{III}, Al^{III}, Y^{III}, and Lu^{III} ($\lambda_{max} \approx 510$ and 700 nm; see Table 1).[11] However, when we prepared the $[Mn^{IV}(O)(dpaq)]^+$–Lewis-acid adducts in MeCN according to published procedures,[11] we observed the absorption intensities of these complexes to be a factor of 10 higher than those of **1**-Sc^{III} (Table 1 and Figure S2). On the basis of this difference, as well as additional spectroscopic data described below, we can conclude that **1**-Sc^{III} does not correspond to $[Mn^{IV}(O)(dpaq)]^+$–Sc^{III}. Due to the slow formation of **1**-Sc^{III} at room temperature, the intermediate was also formed at 50 °C, where the reaction reaches a maximum at approximately 1500 s. This significantly enhanced rate of formation facilitated the kinetic studies below.

When 2 equiv of $Al(OTf)_3$ are added to **1** dissolved in a 99:1 (v:v) MeCN:H_2O solution at 50 °C, we observe the formation of electronic absorption bands at 350, 410, 510, and 700 nm (Figure 2). This resulting chromophoric species will be referred to as **1**-Al^{III}. The position and intensities of the electronic absorption bands of **1**-Al^{III} are nearly identical to those of **1**-Sc^{III} (Table 1), although the dip in absorbance near 600 nm is better resolved for **1**-Al^{III}. As in the case of **1**-Sc^{III}, the formation of **1**-Al^{III} reaches a maximum approximately 1500 s after the addition of $Al(OTf)_3$ to **1**. Investigations of the reaction of **1** with the milder Lewis acids $Ca(OTf)_2$ and $Y(OTf)_3$ failed to result in any significant spectral changes (Figure S3), suggesting no reaction of the Mn^{III}–hydroxo complex with these Lewis acids under these conditions.

Characterization of 1-Sc^{III} and 1-Al^{III} by ^{1}H NMR Measurements. The ^{1}H NMR spectra for **1**-Sc^{III} and **1**-Al^{III}, which were prepared using methods employed for the electronic absorption experiments but using deuterated solvents (98:2 MeCN-d_3:D_2O), are shown in Figure 3. The ^{1}H NMR spectrum of Mn^{III}–hydroxo **1**, in the absence of any

Table 1. Electronic Absorption and Mn K-edge X-ray Absorption Properties for $[Mn^{III}(OH)(dpaq)]^+$ (1), $[Mn^{III}(OH)(dpaq)]^+$ in the Presence of 2 equiv of $Sc(OTf)_3$ (1-Sc^{III}) and $Al(OTf)_3$ (1-Al^{III}), $[Mn^{III}(OH_2)(dpaq)]^{2+}$ (1-H^+), and $[Mn^{IV}(O)(dpaq)]^+$–Sc^{III}

compd	λ (nm)	ε (M^{-1} cm^{-1})	pre-edge energy (eV)	edge energy (eV)
1	385	3190	6540.2	6550.6
	500	280	6541.8	
	770	110		
1-Sc^{III}	350	3510	6540.3	6550.6
	410	2450	6541.9	
	510	380		
	700	300		
	1150[a]	60[a]		
1-Al^{III}	350	3540	ND[b]	ND[b]
	410	2830		
	712	300		
	1150[a]	60[a]		
1-H^+[c]	350	3530	ND[b]	ND[b]
	410	2460		
	510	300		
	718	260		
$[Mn^{IV}(O)(dpaq)]^+$–Sc^{III}[d]	510	2720	NR[e]	NR[e]
	700	2910		

[a]This band is weak and its position and extinction coefficient are not precisely defined (Figure S1). [b]Not determined (ND). [c]Prepared according to the procedure in ref 10, with the exception that $HClO_4$ was used instead of HOTf. [d]Prepared according to the procedure in ref 11. [e]Although Mn K-edge X-ray absorption data for this complex are available,[11] the pre-edge and edge energies were not reported (NR). The Mn K-edge of $[Mn^{IV}(O)(dpaq)]^+$–Sc^{III} appears to be at least 1 eV higher in energy than that of **1**, while the pre-edge transition energy seems comparable.

https://dx.doi.org/10.1021/acs.inorgchem.9b02980
Inorg. Chem. 2020, 59, 2689–2700

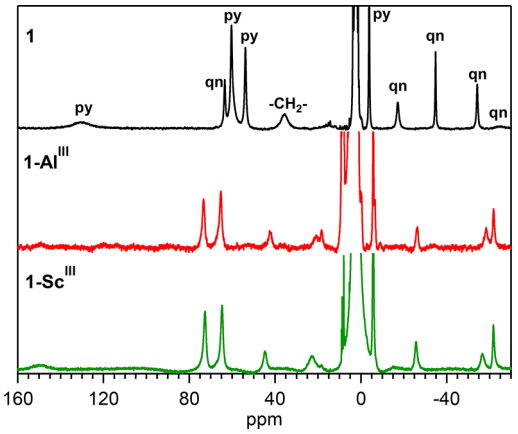

Figure 3. ^{1}H NMR spectra of 2 mM $[Mn^{III}(OH)(dpaq)]^+$ (**1**) dissolved in 98:2 MeCN-d_3:D_2O (top) and $[Mn^{III}(OH)(dpaq)]^+$ in 98:2 MeCN-d_3:D_2O (v:v) in the presence of 2 equiv of $Al(OTf_3)$ (**1**-Al^{III}; center) and 2 equiv of $Sc(OTf)_3$ (**1**-Sc^{III}; bottom).

Lewis acids, is also included in Figure 3 and will be summarized to provide a point of comparison. The ^{1}H NMR spectrum of **1** in 98:2 MeCN-d_3:D_2O shows 10 hyperfine-shifted peaks from 131 to −64 ppm (Figure 3, top). Tentative assignments for many of these resonances have come from previous ^{1}H NMR investigations of **1**, $[Mn^{III}(OH)(dpaq^{5\text{-}R})]^+$ derivatives, and the Mn^{III}−methoxy complex $[Mn^{III}(OMe)(dpaq)]^+$.[12,35] The quinolinyl protons for **1** give rise to the upfield resonances from −15 to −63 ppm and the downfield resonance at 63 ppm, while pyridyl protons are responsible for the resonances at 130, 61, 54, and −5 ppm. The resonance at 40.5 ppm most likely arises from a backbone -CH_2- group.

The ^{1}H NMR spectrum for **1**-Sc^{III} is shown in Figure 3 (bottom). This spectrum bears a strong resemblance to that of **1**. Although the chemical shifts for the proton resonances of **1**-Sc^{III} are perturbed slightly relative to those of **1**, the ^{1}H NMR spectra of **1** and **1**-Sc^{III} display the same number of upfield- and downfield-shifted resonances (Figure 3 and Table 2). Significant shifts in the upfield-shifted peaks associated with the quinoline are observed for **1**-Sc^{III} (Figure 3). The sharp peak at −33 ppm for **1** is shifted and could potentially correspond to one of the two furthest upfield peaks for **1**-Sc^{III}. The broad quinoline peak at −63.4 ppm for **1** could correspond to the broad, weak feature at −15.3 ppm in the spectrum of **1**-Sc^{III}. The similarities between the ^{1}H NMR spectra of **1** and **1**-Sc^{III} extend to the line shapes, which are comparable between the two spectra (Figure 3). Taken together, these spectral similarities suggest that the molecular symmetries of **1** and **1**-Sc^{III} are quite similar. These similarities would preclude significant interaction between Sc^{III} and the pyridine groups of the dpaq ligand in **1**-Sc^{III}, as that would split the pyridine resonances into non-equivalent environments. Moreover, the data provide strong evidence that the dpaq ligand remains coordinated to the Mn^{III} center in the presence of Sc^{III}.

The ^{1}H NMR spectrum of **1**-Al^{III} is nearly identical to that of **1**-Sc^{III} (Figure 3, center and bottom). The spectra for these samples show virtually no variation in chemical-shift values (Table 2). The only notable difference between these spectra is the inability to resolve resonances near 149 and −15.3 ppm for **1**-Al^{III} (Figure 3). These peaks are the broadest peaks observed for **1**-Sc^{III} and might be unobservable for **1**-Al^{III} due to the lower signal-to-noise ratio for this sample. In any case, the near-identical appearances of the ^{1}H NMR spectra of **1**-Sc^{III} and **1**-Al^{III} indicate near-identical environments for the Mn^{III} centers in these samples.

X-ray Absorption Spectroscopy of 1-Sc^{III}. The X-ray absorption near-edge spectra (XANES) for $[Mn^{II}(dpaq)](OTf)$ in MeCN, **1**, and **1**-Sc^{III} are shown in Figure 4. The K-edge energy serves as a probe for the oxidation state of the Mn center, with shifts of 1 eV or greater to higher energy indicative of an increase in oxidation state. The edge energy of **1**-Sc^{III} (which is defined here as the inflection point of the rising edge and is identified by the second derivative of the spectra) is

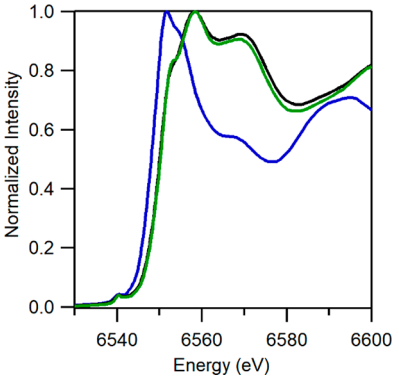

Figure 4. Normalized X-ray absorption spectra for $[Mn^{II}(dpaq)](OTf)$ in MeCN (blue), **1** (black), and **1**-Sc^{III} (green) near the Mn K-edge. Data for $[Mn^{II}(dpaq)](OTf)$ in MeCN and **1** are from ref 38.

Table 2. ^{1}H NMR Chemical Shifts for $[Mn^{III}(OH)(dpaq)]^+$ (1), $[Mn^{III}(OH)(dpaq)]^+$ in the Presence of 2 Equiv of $Sc(OTf)_3$ (1-Sc^{III}) and $Al(OTf)_3$ (1-Al^{III}), and $[Mn^{III}(OH_2)(dpaq)]^{2+}$ (1-H^+) in 98:2 (v:v) MeCN-d_3:D_2O

	chemical shift (ppm)			
tentative assignment	**1**	**1**-Sc^{III}	**1**-Al^{III}	**1**-H^+
H-py	130.5	149		
H-qn	62.7	72.7	73.4	71.0
H-py	60.9	64.7	66.0	63.2
H-py	54.3	44.7	42.6	44.4
	40.5	22.6 (18.2, sh)	20.8 (18.3, sh)	22.5 (17.9, sh)
H-py	−4.6	−5.7	−5.4	−5.5
H-qn	−15.5	−15.3		
H-qn	−33.7	−25.7	−25.9	−25.0
H-qn	−53.8	−56.8	−58.6	−55.0
H-qn	−63.4	−61.8	−61.9	−60.3

https://dx.doi.org/10.1021/acs.inorgchem.9b02980
Inorg. Chem. 2020, 59, 2689−2700

6550.6 eV. This value is identical to that previously reported for **1** and greater than that of $[Mn^{II}(dpaq)](OTf)$ in MeCN frozen solution (Figure 4 and Table 1), which demonstrates that **1**-Sc^{III} retains the Mn^{III} oxidation state. In the study of the Lewis-acid adduct of the $[Mn^{IV}(O)(dpaq)]^+$ complex, a pronounced blue shift for the Mn K-edge was noted,[11] further confirming that **1**-Sc^{III} does not correspond to $[Mn^{IV}(O)(dpaq)]^+$–Sc^{III}. The rest of the XANES region for **1**-Sc^{III}, including the pre-edge and immediate postedge regions, also show little perturbation from **1** (Figure 4 and Table 1).

Structural Properties of 1-Sc^{III} from EXAFS Data. Further insight into the structural properties of **1**-Sc^{III} were obtained by fitting the EXAFS parameters for this complex (Figure 5). Parameters obtained from fits of the $k^3\chi(k)$ data

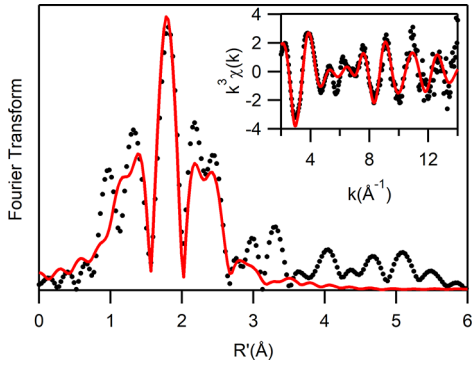

Figure 5. Fourier transform of Mn K-edge EXAFS data and raw EXAFS curve (inset) for **1**-Sc^{III} with experimental (dotted lines) and fit (solid lines). Parameters for the fit are bolded and italicized in Table S1.

collected for **1**-Sc^{III} are shown in Table S1. The best fit, as determined by the reduced χ^2, is bolded and italicized. In this fit, there is an inner O/N shell at 1.92 Å with a degeneracy of 2 and an outer shell of N scatterers at 2.18 Å with a degeneracy of 4. The best fit also includes a C shell, arising from nearby carbons of the dpaq ligand, with a distance of 2.94 Å. The parameters from this fit of **1**-Sc^{III} suggest that the coordination environment has not changed significantly from **1** upon the addition of Sc^{3+} (Table 3). Compared to EXAFS fitting results

Table 3. Comparison of the Parameters Derived from the Best EXAFS Fits for 1 and 1-Sc^{III}

complex	path	n	R (Å)	$\sigma^2 \times 10^3$
1[a]	O/N	2	1.87	4.81
	N	4	2.14	5.21
	C	6	2.91	8.89
1-Sc^{III}	O/N	2	1.92	6.32
	N	4	2.18	5.87
	C	6	2.94	4.84

[a]Values from ref 38.

for **1**, the distance of the nearest O/N shell of **1**-Sc^{III} has increased by 0.05 Å, and the distance for the outer N shell has increased by 0.04 Å.[39]

The analysis of EXAFS data provides no evidence of an interaction between the Sc^{III} ion and the Mn^{III}–hydroxo complex. In a μ-oxoiron(III)scandium(III) complex, Que and co-workers observed a large peak in the Fourier transform beyond 3 Å due to the O-bound Sc^{III} ion.[13] The lack of such a prominent feature beyond 3 Å in the Fourier transform of **1**-Sc^{III} could suggest that the Sc^{III} is not bound to the hydroxo ligand.

Hydrocarbon Oxidation by 1-Sc^{III} and 1-Al^{III}. The effects of $Sc(OTf)_3$ and $Al(OTf)_3$ on the reactivity of the Mn^{III}–hydroxo unit was determined by investigating the reactivity of **1**-Sc^{III} and **1**-Al^{III} with hydrocarbons. The parent complex, **1**, shows only a limited ability to oxidize C–H bonds.[8] Upon addition of excess (>10 equiv) 9,10-dihydroanthracene (DHA) to **1**-Sc^{III} at 50 °C, the optical signals decay by a pseudo-first-order process, which can be fit to yield a k_{obs} value (Figure 6, top). A plot of k_{obs} as a function of DHA

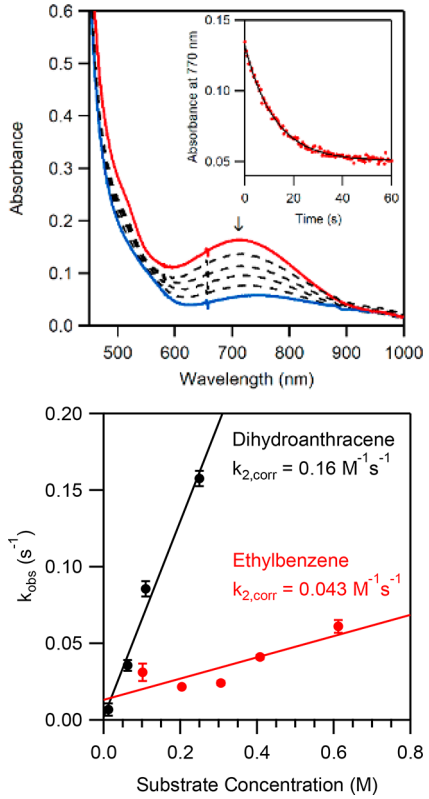

Figure 6. (Top) Electronic absorption spectrum of 1.25 mM **1**-Sc^{III} in 2 mL of 99:1 (v:v) MeCN:H_2O before (red trace) and after (dashed black and solid blue traces) addition of 100 equiv of DHA. Inset shows the decay of the 700 nm electronic absorption signal as a function of time. (Bottom) Plot of k_{obs} as a function of substrate concentration for DHA (black) and ethylbenzene (red).

concentration is linear and yields a corrected second-order rate constant ($k_{2,corr}$; where the correction pertains to the number of abstractable C–H bonds) of 0.16(1) M^{-1} s^{-1} (Figure 6, bottom). Notably, **1** shows no reactivity with DHA. Indeed, the only Mn^{III}–OH complex that is currently known to react with DHA is $[Mn^{III}(OH)(PY5)]^{2+}$, which had a $k_{2,corr}$ of 0.0055 M^{-1} s^{-1} at 50 °C in MeCN.[6] The 30-fold faster rate of **1**-Sc^{III} demonstrates the ability of a redox inactive Lewis acid to greatly increase the reactivity of the complex and allows for reactions with substrates of bond strengths that were previously inaccessible.

The ability of **1**-Sc^{III} to oxidize C–H bonds stronger than those of DHA (BDFE of 76 kcal mol^{-1})[40] was explored. The addition of excess ethylbenzene (BDFE = 87 kcal mol^{-1})[40] to **1**-Sc^{III} at 50 °C led to the disappearance of the optical signal at

https://dx.doi.org/10.1021/acs.inorgchem.9b02980
Inorg. Chem. 2020, 59, 2689–2700

Scheme 2. Possible Structures for 1-Sc^{III}, Featuring Direct Sc^{III} Binding (A) or Protonation Due to the Acidity of the Sc^{III}–Aqua Adduct (B)

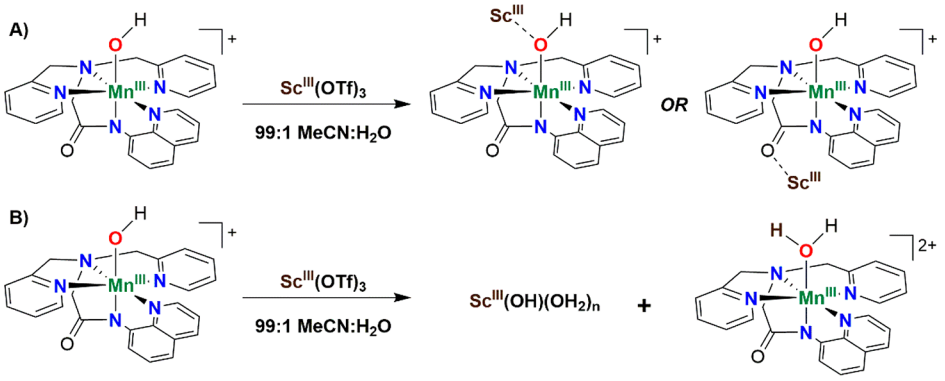

700 nm. This disappearance followed psudo-first-order behavior, and a plot of k_{obs} values versus ethylbenzene concentration permitted the determination of a corrected second-order rate constant of 0.043(3) M^{-1} s^{-1} (Figure 6, bottom). The decrease in reaction rate of **1**-Sc^{III} with the stronger C–H bond of ethylbenzene is in line with the Bell–Evans–Polayni relation, where reactions with lower thermodynamic driving forces display slower reaction rates.

To determine the effect of Lewis-acid identity on the rate of C–H bond oxidation, we performed complementary investigations of DHA oxidation by **1**-Al^{III}. The electronic absorption bands of **1**-Al^{III} showed pseudo-first-order decay behavior upon the addition of DHA, and an analysis of a plot of k_{obs} versus DHA concentration yields a second-order rate constant ($k_{2,corr}$) of 0.25(2) M^{-1} s^{-1} (Figure S4). Thus, the rates of DHA oxidation of **1**-Sc^{III} and **1**-Al^{III} are very similar. Previous investigations of hydrocarbon oxidation by [Mn^{IV}(O)(dpaq)]$^+$–Lewis-acid adducts found the [Mn^{IV}(O)(dpaq)]$^+$–Sc^{III} and [Mn^{IV}(O)(dpaq)]$^+$–Al^{III} complexes to have rates for cyclohexadiene oxidation that were virtually identical (0.016(1) and 0.018(1) M^{-1} s^{-1} at −20 °C, respectively).[11]

The reaction of **1**-Sc^{III} with DHA yields multiple oxidation products of DHA. In total, we observe 0.40 equiv of anthracene, 0.30 equiv of anthrone, 0.23 equiv of 9,10-dihydroanthracene-9-ol, and 0.07 equiv of anthraquinone relative to the starting Mn^{III} concentration (Figure S5). These products are consistent with an initial hydrogen atom abstraction from DHA by **1**-Sc^{III} that yields a monohydroanthracene radical. This radical then undergoes subsequent decay reactions, several of which involve trapping by dioxygen, to give the observed products. This distribution of organic products contrasts with that reported for DHA oxidation by Mn^{IV}-oxo and Mn^{III}-oxo centers, where ca. 0.50 equiv of anthracene has been observed for each equivalent of Mn-oxo complex.[9,41]

The electronic absorption spectrum of the product solution reveals a weak band centered near 710 nm (Figure 6, top). The [Mn^{II}(dpaq)(NCMe)]$^+$ complex, which is an expected product of the reaction, shows only a weak electronic absorption band at 510 nm (ε = 130 $M^{-1}cm^{-1}$),[8] and thus this complex cannot account for the 710 nm feature. The absorption spectrum of [Mn^{II}(dpaq)](OTf) in a 98:2 (v:v) MeCN:H$_2$O solution in the presence of 2 equiv of Sc(OTf)$_3$ likewise shows no features near 710 nm (Figure S6). Because the electronic absorption data do not offer clear insight into the nature of the Mn product, we attempted to characterize this product using EPR and ^{1}H NMR spectroscopies. The EPR spectrum of the product solution reveals a six-line signal centered near g = 2.00 (Figure S7). This EPR signal is distinct from that of [Mn^{II}(dpaq)](OTf) in a 98:2 (v:v) MeCN:H$_2$O solution with 2 equiv of Sc(OTf)$_3$ but resembles that previously reported for the aquated Mn^{II} ion.[42] Spin quantification reveals that this signal can account for only 20% of the Mn in the solution. ^{1}H NMR investigation of the product solution reveals the disappearance of signals associated with **1**-Sc^{III} and the appearance of a small set of new hyperfine-shifted peaks (Figure S8). These signals, which presumably arise from some Mn^{III} species distinct from **1** and **1**-Sc^{III}, could arise from oxidation of the Mn^{II} product and/or from the product of some side reaction.

Possible Formulations for 1-Sc^{III} and Al^{III}. The spectroscopic data collected for **1**-Sc^{III} and Al^{III} clearly establish a perturbation in the geometric and electronic structures of these complexes relative to the Mn^{III}–hydroxo species **1**. ^{1}H NMR data for **1**-Sc^{III} and Al^{III} show large signal shifts relative to **1**, but, at least for **1**-Sc^{III}, the number of signals observed requires that the Mn^{III} center in this complex maintains the same symmetry as that in the Mn^{III}–hydroxo complex **1**. This result is consistent with an interaction between Sc^{III} and either the hydroxo moiety or the oxygen of the amide trans to the hydroxo (Scheme 2A). Because of the nearly identical ^{1}H NMR spectra of **1**-Sc^{III} and **1**-Al^{III}, a similar interaction with Al^{III} could be presumed. Binding a Lewis acid to either the hydroxo or amide carbonyl function would be expected to result in elongation of the axial Mn–ligand bonds, which is supported by the EXAFS parameters for **1**-Sc^{III} (Table 3) and the electronic absorption signals of **1**-Sc^{III}. By analogy to other six-coordinate Mn^{III} complexes,[43] the 1150 nm absorption band of **1**-Sc^{III} can be attributed to a Mn^{III} $3d_{x^2-y^2} \rightarrow 3d_{z^2}$ one-electron excitation, where the z-axis lies along the N_{amide}–Mn–OH vector, and the x- and y-axes are roughly coincident with the equatorial Mn–N bond axes. The red shift in this band compared to that of **1** (780 nm) is consistent with stabilization of the Mn^{III} $3d_{z^2}$ acceptor MO through axial elongations. The lack of a signature metal–metal scatterer peak in the Fourier transform of the EXAFS data for **1**-Sc^{III} suggests that Sc^{3+} is not bound to the hydroxo ligand. However, this result does not provide definitive support that the Sc^{3+} is binding to the amide oxygen. Lewis-acid binding to the carbonyl oxygen of the dpaq ligand would result in a Mn···

https://dx.doi.org/10.1021/acs.inorgchem.9b02980
Inorg. Chem. 2020, 59, 2689–2700

Lewis-acid scattering distance of ca. 6 Å, which would be challenging to detect from EXAFS data.

Given that the spectroscopic data collected for **1**-Sc^{III} fail to provide any evidence for a direct interaction between the Sc^{III} ion and the Mn^{III}–hydroxo complex, there is an alternative proposal to consider due to the presence of significant H_2O in solution. The addition of $Sc(OTf)_3$ to the 99:1 (v:v) MeCN:H_2O solution should result in the formation of Sc^{III}–aqua species. Given that $[Sc(OH_2)_6]^{3+}$ has a pK_a of 4.3–4.8,[44,45] a Sc^{III}–aqua adduct could protonate the Mn^{III}–hydroxo complex **1**, likely forming the previously reported Mn^{III}–aqua species $[Mn^{III}(OH_2)(dpaq)]^+$ (Scheme 2B). The reported pK_a for $[Mn^{III}(OH_2)(dpaq)]^{2+}$ (6.78 in MeCN) suggests this process would be thermodynamically favorable.[10]

Comparison of 1-Sc^{III} and 1-Al^{III} with $[Mn^{III}(OH_2)(dpaq)]^{2+}$ (1-H^+). To compare the spectroscopic properties of **1**-Sc^{III} and **1**-Al^{III} to those of the Mn^{III}–aqua species $[Mn^{III}(OH_2)(dpaq)]^{2+}$, we independently prepared the latter by treating **1** with $HClO_4$ in 99:1 (v:v) MeCN:H_2O. With this approach, we rely on the previous work of Nam and co-workers that established that the reaction of **1** with strong acid leads to the protonation of the hydroxo ligand.[10] We first verified the formation of $[Mn^{III}(OH_2)(dpaq)]^{2+}$ on the basis of the reported electronic absorption band maxima and intensities in the UV region. Treatment of a 0.25 mM solution of **1** with 1 equiv of $HClO_4$ in MeCN at 50 °C led to the appearance of new electronic absorption bands at 350 and 410 nm (Figure 7, top), which are identical to those reported previously for $[Mn^{III}(OH_2)(dpaq)]^{2+}$ (λ_{max} = 350 and 410 nm in MeCN at 25 °C).[10] A 0.25 mM sample of **1**-Sc^{III} was prepared to compare the near-UV features of this sample with that of **1**-H^+. As seen in Figure 6 (bottom), **1**-Sc^{III} shows near-UV bands with positions and intensitites indistinguishable from those of **1**-H^+ (see also Table 1). Electronic absorption spectra of more concentrated (1.25 mM) solutions of **1**-Sc^{III} and **1**-H^+ likewise reveal very similar optical features in the visible region (Figure 6, bottom).

As a further means of comparing **1**-Sc^{III} and **1**-H^+, we collected ^{1}H NMR data for the latter complex in 98:2 (v:v) MeCN-d_3:D_2O. The ^{1}H NMR spectrum of $[Mn^{III}(OH_2)(dpaq)]^+$ is virtually identical to that of **1**-Sc^{III} (Figure 8). In particular, the hyperfine-shifted resonances for these samples display chemical shifts that differ by less than 2 ppm (Table 2). Thus, both electronic absorption ^{1}H NMR data provide strong evidence that treatment of $[Mn^{III}(OH)(dpaq)]^+$ with Sc^{III} in wet MeCN results in the formation of the $[Mn^{III}(OH_2)(dpaq)]^+$ species. Since the spectroscopic data for **1**-Sc^{III} and **1**-Al^{III} are nearly identical, we can also conclude that the addition of Al^{III} to **1** likewise results in the formation of the Mn^{III}–aqua complex **1**-H^+. This formulation also explains a lack of reactivity of **1** with milder Lewis acids, such as $Ca(OTf)_2$ and $Y(OTf)_3$ (Figure S3); these Lewis acids are not sufficiently acidic to cause protonation of the Mn^{III}–hydroxo adduct.

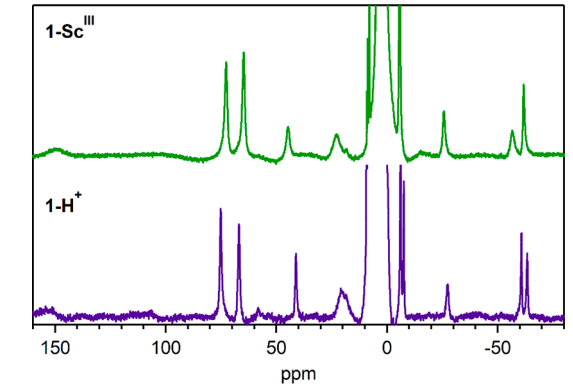

Figure 8. ^{1}H NMR spectra of 2 mM **1**-Sc^{III} in MeCN-d_3 in 99:1 (top) and 2.5 mM **1**-H^+ in 98:2 (v:v) MeCN-d_3:D_2O.

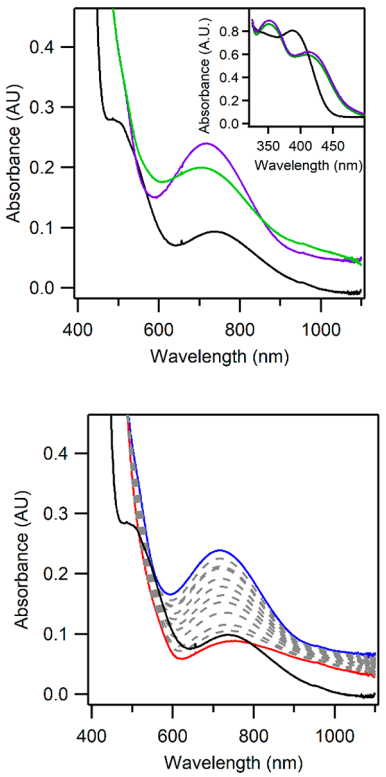

Figure 7. (Top) Overlay of the electronic absorption spectra for $[Mn^{III}(OH_2)(dpaq)]^{2+}$ (purple trace) and **1**-Sc^{III} (green trace). The electronic absorption spectrum of **1** (black trace) is included for comparison. (Bottom) Electronic absorption spectra showing the optical changes observed after the addition of 1 equiv of $HClO_4$ to **1** in 99:1 (v:v) MeCN:H_2O at 50 °C.

In further support of this proposal, treatment of **1**-Sc^{III} and **1**-Al^{III} with 3 equiv of triethylamine causes the electronic absorption features of these species to revert to those of the Mn^{III}–hydroxo adduct **1** (Figure S9). This chemistry thus matches that reported for $[Mn^{III}(OH_2)(dpaq)]^{2+}$ upon treatment with base.[10] In addition, the $[Mn^{IV}(O)(dpaq)]^+$–Al^{III} adduct, prepared using a previously reported method,[11] shows no reaction with 3 equiv of triethylamine (Figure S9), further confirming that the visible absorption features of **1**-Al^{III} do not arise from a small amount of the Mn^{IV}–oxo complex.

This assignment of **1**-Sc^{III} as **1**-H^+ is also consistent with the metric parameters of **1**-Sc^{III} that were obtained from an analysis of the EXAFS data (Table 3). The Mn–ligand distances from the crystal structure of $[Mn^{III}(OH_2)(dpaq)]^{2+}$ would correspond to an n = 2 O/N shell at 1.93 Å (from the hydroxo and amide functions) and an n = 4 N shell at 2.16 Å (from the pyridine, quinoline, and amine functions).[10] The distances for these shells agree very well with the parameters derived from the EXAFS fit for **1**-Sc^{III} (1.92 and 2.18 Å for the O/N and N shells, respectively; see Table 3).

https://dx.doi.org/10.1021/acs.inorgchem.9b02980
Inorg. Chem. 2020, 59, 2689–2700

Comparison of the Reactivity of 1-H$^+$, 1-Sc^{III}, and 1-Al^{III} in Hydrocarbon Oxidation. To evaluate our prediction that the addition of Sc^{III} and Al^{III} to **1** result in the formation of the Mn^{III}–aqua complex **1**-H$^+$, we explored the reactivity of the latter complex with DHA and ethylbenzene. (A previous investigation of the reactivity of **1**-H$^+$ focused on its ability to oxidize the O–H bonds of phenolic substrates; reactions of **1**-H$^+$ with hydrocarbons were not reported.[10]) The reaction of **1**-H$^+$ with excess DHA in 99:1 (v:v) MeCN:H_2O at 50 °C follows pseudo-first-order behavior (Figure 9). Experiments

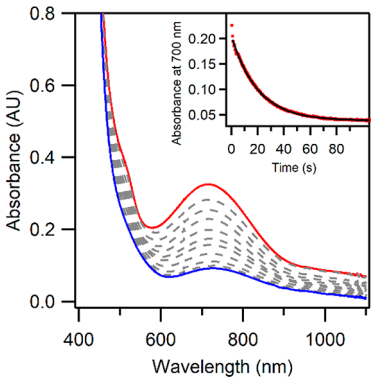

Figure 9. Electronic absorption spectrum of 1.25 mM **1**-H$^+$ in 2 mL of 99:1 (v:v) MeCN:H_2O before (red trace) and after (blue trace) the addition of 50 equiv of DHA. Inset shows the decay of the 700 nm electronic absorption signal as a function of time.

using different DHA concentrations allow us to determine a second-order rate constant for DHA oxidation by **1**-H$^+$ of 0.19(1) M^{-1} s^{-1} (Figure 10). This rate is identical, within

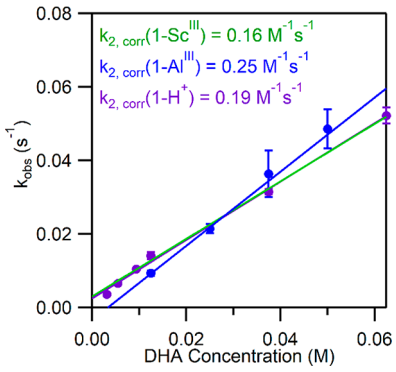

Figure 10. Plot of k_{obs} for the reaction of **1**-Sc^{III} (green points), **1**-Al^{III} (blue points) and **1**-H$^+$ (purple points) with DHA as a function of DHA concentration.

error, to the rates of DHA oxidation by **1**-Sc^{III} and **1**-Al^{III} (Figure 10). In addition, an analysis of organic products following the reaction of DHA with **1**-H$^+$ shows the formation of a mixture of oxidized derviatives of DHA, whose ratios are essentially identical to that observed for DHA oxidation by **1**-Sc^{III} (Figure S10). The similarities in rates and product yields for DHA oxidation by **1**-Sc^{III} and **1**-H$^+$ support the notion that the oxidant formed is the same in each case.

Possible Alternative Formulation for the Product of 1 with Protons and Lewis Acids. In the formulation of the product of the reaction of **1** with H$^+$ (and, by analogy, Sc^{III}(OTf)$_3$ and Al^{III}(OTf)$_3$), we have relied on the previous solid-state structure of [Mn^{III}(OH$_2$)(dpaq)]$^{2+}$.[10] Since solid-state structures are not always representative of solution-phase composition, we have considered an alternative structure given the relative basicities of the coordinating ligands. The amide nitrogen of the dpaq ligand is quite basic and represents an alternative site for protonation of **1**.[46] Protonation at this position would be expected to cause a large rearrangement of the dpaq ligand. An X-ray structure of [Mn^{II}(Cl$_2$)(dpaqH)] provides a model for metal coordination by the protonated dpaqH ligand (Figure 11).[47] For [Mn^{II}(Cl$_2$)(dpaqH)], the

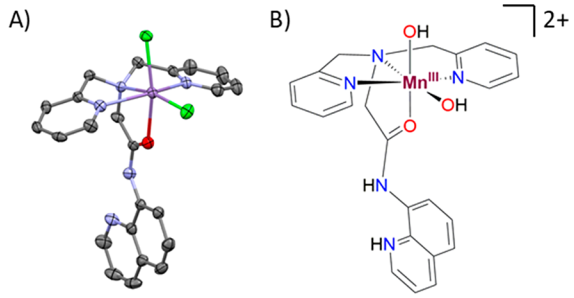

Figure 11. (A) ORTEP rendering of the X-ray diffraction structure of [Mn^{II}(Cl$_2$)(dpaqH)] with hydrogen atoms omitted for clarity.[47] (B) Potential structure of [Mn^{III}(OH)$_2$(dpaq)]$^{2+}$.[46]

dpaqH ligand is coordinated in a tetradentate fashion through the two pyridyl functions, the tertiary amine and the carbonyl oxygen. The quinolinyl arm is noncoordinating.[47] In the case of the reaction of **1** with protons or Lewis acids in the presence of excess water, dpaq protonation and metal ion coordination in a similar fashion would give two coordination sites that could be occupied by hydroxo ligands (Figure 11). A bis(hydroxo)manganese(III) complex would be a reasonable hydrogen-atom abstraction agent, consistent with the observed chemistry of **1**-H$^+$, **1**-Sc^{III}, and **1**-Al^{III}. Although we interpret the similarities in the ^{1}H NMR spectra of **1**, **1**-H$^+$, **1**-Sc^{III}, and **1**-Al^{III} (Figures 3 and 8) as indicative of a common binding mode for the dpaq ligand, the ^{1}H NMR data do not unambiguously rule out the [Mn^{III}(OH)$_2$(dpaqH)]$^{2+}$ formulation.

We investigated the possibility of amide protonation for these complexes by collecting IR data for solution and solid-state samples of **1** and **1**-Sc^{III}. Unfortunately, the solution-state IR data are dominated by solvent-derived peaks and offer no conclusive evidence for or against the presence of an N–H vibration from an amide group. The dominance of solvent-derived features in the solution-phase IR data also complicates any comparison of solution- and solid-state IR data for **1**-Sc^{III}. A detailed discussion of these IR results is provided in the Supporting Information.

In summary, solution and solid-state IR data cannot be used to discount amide protonation upon the reaction of **1** with H$^+$ in solution. Therefore, this possible alternative formulation may be considered until more fully evaluated. Regardless of the solution-phase structure for the protonated form of **1**, our central finding is the same, namely, that treatment of **1** with strong Lewis acids leads to the same effect as treatment with the Brønsted acid H$^+$. Thus, the primary effect of the Lewis acids in the present case is to coordinate to water and increase the Brønsted acidity of the solution.

https://dx.doi.org/10.1021/acs.inorgchem.9b02980
Inorg. Chem. 2020, 59, 2689–2700

CONCLUSIONS AND PERSPECTIVE

Several biological catalysts, such as CuZn superoxide dismutase (CuZnSOD) and the oxygen-evolving complex of photosystem II, utilize Lewis acids to modulate the properties and chemical reactivity of redox-active metal centers.[48,49] The presence of a Ca^{II} ion in the tetramanganese cluster of the oxygen-evolving complex is critical to the water-splitting activity of this catalyst. Inspired by these observations from biology, there is significant current interest in understanding the influence of Lewis acids on the properties and oxidative reactivity of synthetic transition-metal complexes. In many cases, ligand design is employed to incorporate Lewis basic functional groups capable of binding Lewis acids in positions adjacent to redox-active metal centers.[30,31,50−56] Achievements in this area have shown the profound effect Lewis acids can have on modulating the reduction potentials of adjacent transition metals.

Lewis acids have also been shown to influence the chemical reactivity of transition-metal complexes lacking motifs designed for Lewis-acid binding.[13−28,57−59] In these cases, an interaction of the Lewis acid with a Lewis basic site on the transition metal is commonly presumed; however, detailed spectroscopic or crystallographic characterization of these proposed interactions is often lacking. In such cases the effect of the Lewis acid on chemical reactivity is known, but, given the lack of structural information, the exact cause for this effect is unclear.

In this present study, we have shown that the addition of highly Lewis acidic Sc^{III} and Al^{III} salts to the mononuclear Mn^{III}−hydroxo complex **1** generates new intermediates **1**-Sc^{III} and **1**-Al^{III}. Because the spectroscopic properties of **1**-Sc^{III} and **1**-Al^{III} are perturbed, yet still very similar, to those of **1**, we conclude that these Lewis acids do not cause any gross distortions to the dpaq ligand binding mode. In contrast, the additions of Sc^{III} and Al^{III} have profound effects on the oxidative reactivity of **1**. In the absence of these Lewis acids, **1** is only capable of sluggishly attacking hydrocarbons with very low BDFEs (ca. 73 kcal mol^{-1}). In contrast, in the presence of Sc^{III}, **1** can attack the significantly stronger C−H bond of ethylbenznene. The rate of reaction of **1**-Sc^{III} with DHA (0.16 M^{-1} s^{-1}) exceeds that for DHA oxidation by several Mn^{IV}−oxo adducts at similar temperatures.[60,61]

The influence of Sc^{III} and Al^{III} on the physical properties and reactivity of **1** were readily understood by comparing the spectroscopic properties of **1**-Sc^{III} and **1**-Al^{III} with those of the recently reported Mn^{III}−aqua complex **1**-H^+.[10] The electronic absorption properties of these three complexes are remarkably similar (Figure 7), and the ^{1}H NMR spectra of these species are essentially identical (Figure 8). Accordingly, we propose that the addition of Sc^{III} and Al^{III} to **1** in a 99:1 (v:v) MeCN:H_2O solution increases the Brønsted acidity of the solution, resulting in protonation of the Mn^{III}−hydroxo **1** to give the Mn^{III}−aqua **1**-H^+. (The water is a necessary component of the solvent mixture because of an equilibrium between this Mn^{III}−hydroxo complex and a (μ-oxo)-dimanganese(III,III) analogue; see Scheme 1.) The enhanced oxidative reactivity of **1**-H^+ compared to **1** can be understood on the basis of the very different reduction potentials of these complexes (+1.03 and −0.1 V versus SCE, respectively).[8,10] Thus, the Mn^{III}−aqua species is a far better oxidant than the Mn^{III}−hydroxo analogue, and this difference in thermodynamic driving force can account for the enhanced reactivity toward hydrocarbons. Because previous generation of **1**-H^+ utilized a superacid (triflic acid), the formation of **1**-H^+ reported here represents an alternative synthesis employing milder reagents (Lewis acids).

These present results serve as a counterpoint to previous proposals that strong Lewis acids modulate reactivity primarily through interaction with Lewis basic sites on the metal complex. While direct interactions are certainly possible, and even likely, in some cases, the interaction of strong Lewis acids with water, and, potentially, other protic solvents, will change the Brønsted acidity of the reaction solution. From our investigation of the literature, this mode of Lewis-acid modulation of reactivity has been considered less frequently. An exception is a recent work by Browne and co-workers, who demonstrated that the primary effect of $Sc(OTf)_3$ on the activity of a dimanganese(IV) catalyst was through a modulation of the Brønsted acidity of the solution.[62] Whether these results pertain primarily, or exclusively, to Mn^{III}−hydroxo and dimanganese(IV) systems remains to be seen.

ASSOCIATED CONTENT

Supporting Information

The Supporting Information is available free of charge at https://pubs.acs.org/doi/10.1021/acs.inorgchem.9b02980.

Electronic absorption and ^{1}H NMR spectra of $[Mn^{III}(OH)(dpaq)]^+$ reacted with various Lewis acids, kinetic data for DHA oxidation by $[Mn^{III}(OH)(dpaq)]^+$ in the presence of $Al(OTf)_3$, and ^{1}H NMR and EPR spectra for analysis of oxidation products (PDF)

AUTHOR INFORMATION

Corresponding Author

Timothy A. Jackson − *Department of Chemistry and Center for Environmentally Beneficial Catalysis, The University of Kansas, Lawrence, Kansas 66045, United States;* orcid.org/0000-0002-3529-2715; Phone: (785) 864-3968; Email: taj@ku.edu

Authors

Derek B. Rice − *Department of Chemistry and Center for Environmentally Beneficial Catalysis, The University of Kansas, Lawrence, Kansas 66045, United States*

Elizabeth N. Grotemeyer − *Department of Chemistry and Center for Environmentally Beneficial Catalysis, The University of Kansas, Lawrence, Kansas 66045, United States*

Anna M. Donovan − *Department of Chemistry and Center for Environmentally Beneficial Catalysis, The University of Kansas, Lawrence, Kansas 66045, United States*

Complete contact information is available at: https://pubs.acs.org/10.1021/acs.inorgchem.9b02980

Notes

The authors declare no competing financial interest.

ACKNOWLEDGMENTS

This work was supported by the US NSF (Grant CHE-1900384). The U.S. National Science Foundation (NSF) is acknowledged for funds used to support the purchase of EPR instrumentation (Grant CHE-0946883). Use of the Stanford Synchrotron Radiation Lightsource (SSRL), SLAC National Accelerator Laboratory, is supported by the U.S. Department of Energy, Office of Science, Office of Basic Energy Sciences under Contract No. DE-AC02-76SF00515. The SSRL

Structural Molecular Biology Program is supported by the DOE Office of Biological and Environmental Research, and by the National Institutes of Health (NIH), National Institute of General Medical Sciences (NIGMS; including Grant P41GM103393). The contents of this publication are solely the responsibility of the authors and do not necessarily represent the official views of NIGMS or NIH.

REFERENCES

(1) Su, C.; Sahlin, M.; Oliw, E. H. Kinetics of Manganese Lipoxygenase with a Catalytic Mononuclear Redox Center. *J. Biol. Chem.* **2000**, *275* (25), 18830−18835.
(2) Su, C.; Oliw, E. H. Manganese Lipoxygenase: PURIFICATION AND CHARACTERIZATION. *J. Biol. Chem.* **1998**, *273* (21), 13072−13079.
(3) Wennman, A.; Oliw, E. H.; Karkehabadi, S.; Chen, Y. Crystal Structure of Manganese Lipoxygenase of the Rice Blast Fungus Magnaporthe oryzae. *J. Biol. Chem.* **2016**, *291*, 8130−8139.
(4) Wennman, A.; Karkehabadi, S.; Oliw, E. H. Kinetic investigation of the rate-limiting step of manganese- and iron-lipoxygenases. *Arch. Biochem. Biophys.* **2014**, *555*−*556* (0), 9−15.
(5) Rice, D. B.; Massie, A. A.; Jackson, T. A. Manganese−Oxygen Intermediates in O−O Bond Activation and Hydrogen-Atom Transfer Reactions. *Acc. Chem. Res.* **2017**, *50* (11), 2706−2717.
(6) Goldsmith, C. R.; Cole, A. P.; Stack, T. D. P. C−H Activation by a Mononuclear Manganese(III) Hydroxide Complex: Synthesis and Characterization of a Manganese-Lipoxygenase Mimic? *J. Am. Chem. Soc.* **2005**, *127* (27), 9904−9912.
(7) Rice, D. B.; Wijeratne, G. B.; Burr, A. D.; Parham, J. D.; Day, V. W.; Jackson, T. A. Steric and Electronic Influence on Proton-Coupled Electron-Transfer Reactivity of a Mononuclear Mn(III)-Hydroxo Complex. *Inorg. Chem.* **2016**, *55* (16), 8110−8120.
(8) Wijeratne, G. B.; Corzine, B.; Day, V. W.; Jackson, T. A. Saturation Kinetics in Phenolic O−H Bond Oxidation by a Mononuclear Mn(III)−OH Complex Derived from Dioxygen. *Inorg. Chem.* **2014**, *53* (14), 7622−7634.
(9) Barman, S. K.; Jones, J. R.; Sun, C.; Hill, E. A.; Ziller, J. W.; Borovik, A. S. Regulating the Basicity of Metal−Oxido Complexes with a Single Hydrogen Bond and Its Effect on C−H Bond Cleavage. *J. Am. Chem. Soc.* **2019**, *141* (28), 11142−11150.
(10) Sankaralingam, M.; Lee, Y.-M.; Karmalkar, D. G.; Nam, W.; Fukuzumi, S. A Mononuclear Non-heme Manganese(III)−Aqua Complex as a New Active Oxidant in Hydrogen Atom Transfer Reactions. *J. Am. Chem. Soc.* **2018**, *140* (40), 12695−12699.
(11) Sankaralingam, M.; Lee, Y.-M.; Pineda-Galvan, Y.; Karmalkar, D. G.; Seo, M. S.; Jeon, S. H.; Pushkar, Y.; Fukuzumi, S.; Nam, W. Redox Reactivity of a Mononuclear Manganese-Oxo Complex Binding Calcium Ion and Other Redox-Inactive Metal Ions. *J. Am. Chem. Soc.* **2019**, *141*, 1324−1336.
(12) Rice, D. B.; Munasinghe, A.; Grotemeyer, E. N.; Burr, A. D.; Day, V. W.; Jackson, T. A. Structure and Reactivity of (μ-Oxo)dimanganese(III,III) and Mononuclear Hydroxomanganese(III) Adducts Supported by Derivatives of an Amide-Containing Pentadentate Ligand. *Inorg. Chem.* **2019**, *58* (1), 622−636.
(13) Prakash, J.; Rohde, G. T.; Meier, K. K.; Jasniewski, A. J.; Van Heuvelen, K. M.; Münck, E.; Que, L. Spectroscopic Identification of an FeIII Center, not FeIV, in the Crystalline Sc−O−Fe Adduct Derived from [FeIV(O)(TMC)]2+. *J. Am. Chem. Soc.* **2015**, *137* (10), 3478−3481.
(14) Park, J.; Morimoto, Y.; Lee, Y.-M.; Nam, W.; Fukuzumi, S. Unified View of Oxidative C−H Bond Cleavage and Sulfoxidation by a Nonheme Iron(IV)−Oxo Complex via Lewis Acid-Promoted Electron Transfer. *Inorg. Chem.* **2014**, *53* (7), 3618−3628.
(15) Draksharapu, A.; Rasheed, W.; Klein, J. E. M. N.; Que, L., Jr. Facile and Reversible Formation of Iron(III)−Oxo−Cerium(IV) Adducts from Nonheme Oxoiron(IV) Complexes and Cerium(III). *Angew. Chem., Int. Ed.* **2017**, *56* (31), 9091−9095.
(16) Miller, C. G.; Gordon-Wylie, S. W.; Horwitz, C. P.; Strazisar, S. A.; Peraino, D. K.; Clark, G. R.; Weintraub, S. T.; Collins, T. J. A Method for Driving O-Atom Transfer: Secondary Ion Binding to a Tetraamide Macrocyclic Ligand. *J. Am. Chem. Soc.* **1998**, *120*, 11540−11541.
(17) Fukuzumi, S.; Ohkubo, K.; Lee, Y.-M.; Nam, W. Lewis Acid Coupled Electron Transfer of Metal−Oxygen Intermediates. *Chem. - Eur. J.* **2015**, *21* (49), 17548−17559.
(18) Yoon, H.; Lee, Y.-M.; Wu, X.; Cho, K.-B.; Sarangi, R.; Nam, W.; Fukuzumi, S. Enhanced Electron-Transfer Reactivity of Nonheme Manganese(IV)−Oxo Complexes by Binding Scandium Ions. *J. Am. Chem. Soc.* **2013**, *135* (24), 9186−9194.
(19) Chen, J.; Lee, Y.-M.; Davis, K. M.; Wu, X.; Seo, M. S.; Cho, K.-B.; Yoon, H.; Park, Y. J.; Fukuzumi, S.; Pushkar, Y. N.; Nam, W. A Mononuclear Non-Heme Manganese(IV)−Oxo Complex Binding Redox-Inactive Metal Ions. *J. Am. Chem. Soc.* **2013**, *135*, 6388−6391.
(20) Baglia, R. A.; Dürr, M.; Ivanović-Burmazović, I.; Goldberg, D. P. Activation of a High-Valent Manganese−Oxo Complex by a Nonmetallic Lewis Acid. *Inorg. Chem.* **2014**, *53* (12), 5893−5895.
(21) Baglia, R. A.; Krest, C. M.; Yang, T.; Leeladee, P.; Goldberg, D. P. High-Valent Manganese−Oxo Valence Tautomers and the Influence of Lewis/Brönsted Acids on C−H Bond Cleavage. *Inorg. Chem.* **2016**, *55* (20), 10800−10809.
(22) Bougher, C. J.; Abu-Omar, M. M. Lewis-Acid-assisted Hydrogen Atom Transfer to Manganese(V)-Oxo Corrole through Valence Tautomerization. *ChemistryOpen* **2016**, *5* (6), 522−524.
(23) Bougher, C. J.; Liu, S.; Hicks, S. D.; Abu-Omar, M. M. Valence Tautomerization of High-Valent Manganese(V)-Oxo Corrole Induced by Protonation of the Oxo Ligand. *J. Am. Chem. Soc.* **2015**, *137* (45), 14481−14487.
(24) Leeladee, P.; Baglia, R. A.; Prokop, K. A.; Latifi, R.; de Visser, S. P.; Goldberg, D. P. Valence Tautomerism in a High-Valent Manganese−Oxo Porphyrinoid Complex Induced by a Lewis Acid. *J. Am. Chem. Soc.* **2012**, *134* (25), 10397−10400.
(25) Sharma, N.; Jung, J.; Ohkubo, K.; Lee, Y.-M.; El-Khouly, M. E.; Nam, W.; Fukuzumi, S. Long-Lived Photoexcited State of a Mn(IV)-Oxo Complex Binding Scandium Ions That is Capable of Hydroxylating Benzene. *J. Am. Chem. Soc.* **2018**, *140* (27), 8405−8409.
(26) Zaragoza, J. P. T.; Baglia, R. A.; Siegler, M. A.; Goldberg, D. P. Strong Inhibition of O-Atom Transfer Reactivity for MnIV(O)(π-Radical-Cation)(Lewis Acid) versus MnV(O) Porphyrinoid Complexes. *J. Am. Chem. Soc.* **2015**, *137* (20), 6531−6540.
(27) Kanady, J. S.; Mendoza-Cortes, J. L.; Tsui, E. Y.; Nielsen, R. J.; Goddard, W. A.; Agapie, T. Oxygen Atom Transfer and Oxidative Water Incorporation in Cuboidal Mn3MOn Complexes Based on Synthetic, Isotopic Labeling, and Computational Studies. *J. Am. Chem. Soc.* **2013**, *135* (3), 1073−1082.
(28) Chen, Z.; Yang, L.; Choe, C.; Lv, Z.; Yin, G. Non-redox metal ion promoted oxygen transfer by a non-heme manganese catalyst. *Chem. Commun.* **2015**, *51* (10), 1874−1877.
(29) Liu, Y.; Lau, T.-C. Activation of Metal Oxo and Nitrido Complexes by Lewis Acids. *J. Am. Chem. Soc.* **2019**, *141* (9), 3755−3766.
(30) Chantarojsiri, T.; Reath, A. H.; Yang, J. Y. Cationic Charges Leading to an Inverse Free-Energy Relationship for N−N Bond Formation by MnVI Nitrides. *Angew. Chem., Int. Ed.* **2018**, *57* (43), 14037−14042.
(31) Chantarojsiri, T.; Ziller, J. W.; Yang, J. Y. Incorporation of redox-inactive cations promotes iron catalyzed aerobic C−H oxidation at mild potentials. *Chem. Sci.* **2018**, *9* (9), 2567−2574.
(32) Karmalkar, D. G.; Sankaralingam, M.; Seo, M. S.; Ezhov, R.; Lee, Y.-M.; Pushkar, Y. N.; Kim, W.-S.; Fukuzumi, S.; Nam, W. A High-Valent Manganese(IV)−Oxo−Cerium(IV) Complex and Its Enhanced Oxidizing Reactivity. *Angew. Chem.* **2019**, *131*, 16270−16275.
(33) Biswas, S.; Mitra, A.; Banerjee, S.; Singh, R.; Das, A.; Paine, T. K.; Bandyopadhyay, P.; Paul, S.; Biswas, A. N. A High Spin Mn(IV)-Oxo Complex Generated via Stepwise Proton and Electron Transfer

https://dx.doi.org/10.1021/acs.inorgchem.9b02980
Inorg. Chem. 2020, 59, 2689−2700

from Mn(III)−Hydroxo Precursor: Characterization and C−H Bond Cleavage Reactivity. *Inorg. Chem.* **2019**, *58* (15), 9713−9722.
(34) Jensen, M. P.; Costas, M.; Ho, R. Y. N.; Kaizer, J.; Mairata i Payeras, A.; Munck, E.; Que, L., Jr.; Rohde, J.-U.; Stubna, A. High-Valent Nonheme Iron. Two Distinct Iron(IV) Species Derived from a Common Iron(II) Precursor. *J. Am. Chem. Soc.* **2005**, *127* (30), 10512−10525.
(35) Rice, D. B.; Jones, S. D.; Douglas, J. T.; Jackson, T. A. NMR Studies of a MnIII-hydroxo Adduct Reveal an Equilibrium between MnIII-hydroxo and μ-Oxodimanganese(III,III) Species. *Inorg. Chem.* **2018**, *57* (13), 7825−7837.
(36) Ravel, B.; Newville, M. ATHENA, ARTEMIS, HEPHAESTUS: data analysis for X-ray absorption spectroscopy using IFEFFIT. *J. Synchrotron Radiat.* **2005**, *12* (4), 537−541.
(37) Rehr, J. J.; Mustre de Leon, J.; Zabinsky, S. I.; Albers, R. C. Theoretical X-ray Absorption Fine Structure Standards. *J. Am. Chem. Soc.* **1991**, *113*, 5135−5140.
(38) Rice, D. B.; Wijeratne, G. B.; Jackson, T. A. Mn K-edge X-ray absorption studies of mononuclear Mn(III)−hydroxo complexes. *JBIC, J. Biol. Inorg. Chem.* **2017**, *22* (8), 1281−1293.
(39) There is an alternative fit that shows a similar goodness-of-fit as above if evaluated by the *R*-factor (Table S1, italicized). This fit differs from the best fit by separating the O/N shell to give a one-atom O shell at 1.85 Å and two N shells at 2.014 (degeneracy of 2) and 2.18 Å (degeneracy of 3). This fit, however, has one exceptionally low σ^2 value, and the *R*-factor is shown to only be improved due to the inclusion of additional degrees of freedom. Thus, a better comparison between these fits comes from the reduced σ^2, which accounts of the degrees of freedom in the analysis. As such the original fit mentioned above (Table S1, bolded and italicized) is deemed the most reliable fit.
(40) Warren, J. J.; Tronic, T. A.; Mayer, J. M. Thermochemistry of Proton-Coupled Electron Transfer Reagents and its Implications. *Chem. Rev.* **2010**, *110* (12), 6961−7001.
(41) Leto, D. F.; Ingram, R.; Day, V. W.; Jackson, T. A. Spectroscopic properties and reactivity of a mononuclear oxomanganese(iv) complex. *Chem. Commun.* **2013**, *49* (47), 5378−5380.
(42) Groni, S.; Dorlet, P.; Blain, G.; Bourcier, S.; Guillot, R.; Anxolabéhère-Mallart, E. Reactivity of an Aminopyridine $[LMn^{II}]^{2+}$ Complex with H_2O_2. Detection of Intermediates at Low Temperature. *Inorg. Chem.* **2008**, *47* (8), 3166−3172.
(43) Lever, A. B. P. *Inorganic Electronic Spectroscopy*. 2nd ed.; Elsevier: Amsterdam, 1984; pp xvi, 863.
(44) Gilson, R.; Durrant, M. C. Estimation of the pKa values of water ligands in transition metal complexes using density functional theory with polarized continuum model solvent corrections. *Dalton Trans.* **2009**, No. 46, 10223−10230.
(45) Rustad, J. R.; Dixon, D. A.; Rosso, K. M.; Felmy, A. R. Trivalent Ion Hydrolysis Reactions: A Linear Free-Energy Relationship Based on Density Functional Electronic Structure Calculations. *J. Am. Chem. Soc.* **1999**, *121* (13), 3234−3235.
(46) We thank a reviewer, who suggested the possibility of amide protonation and brought to our attention the crystal structure of metal-bound dpaqH in ref 47.
(47) Wang, Z.-W.; Chen, Q.-Y.; Liu, Q.-S. Manganese(II) complexes of quinoline derivatives: characterization, catalase activity, interaction with mitochondria and anticancer activity. *Transition Met. Chem.* **2014**, *39*, 917−924.
(48) Sheng, Y.; Abreu, I. A.; Cabelli, D. E.; Maroney, M. J.; Miller, A.-F.; Teixeira, M.; Valentine, J. S. Superoxide Dismutases and Superoxide Reductases. *Chem. Rev.* **2014**, *114* (7), 3854−3918.
(49) Yano, J.; Yachandra, V. Mn4Ca Cluster in Photosynthesis: Where and How Water is Oxidized to Dioxygen. *Chem. Rev.* **2014**, *114* (8), 4175−4205.
(50) Kumar, A.; Lionetti, D.; Day, V. W.; Blakemore, J. D. Trivalent Lewis Acidic Cations Govern the Electronic Properties and Stability of Heterobimetallic Complexes of Nickel. *Chem. - Eur. J.* **2018**, *24* (1), 141−149.
(51) Sano, Y.; Weitz, A. C.; Ziller, J. W.; Hendrich, M. P.; Borovik, A. S. Unsymmetrical Bimetallic Complexes with M^{II}−(μ-OH)−M^{III} Cores ($M^{II}M^{III}$ = $Fe^{II}Fe^{III}$, $Mn^{II}Fe^{III}$, $Mn^{II}Mn^{III}$): Structural, Magnetic, and Redox Properties. *Inorg. Chem.* **2013**, *52*, 10229−10231.
(52) Sano, Y.; Lau, N.; Weitz, A. C.; Ziller, J. W.; Hendrich, M. P.; Borovik, A. S. Models for Unsymmetrical Active Sites in Metalloproteins: Structural, Redox, and Magnetic Properties of Bimetallic Complexes with M^{II}-(μ-OH)-Fe^{III} Cores. *Inorg. Chem.* **2017**, *56* (22), 14118−14128.
(53) Lau, N.; Sano, Y.; Ziller, J. W.; Borovik, A. S. Modular bimetallic complexes with a sulfonamido-based ligand. *Dalton Trans.* **2018**, *47* (35), 12362−12372.
(54) Kanady, J. S.; Tsui, E. Y.; Day, M. W.; Agapie, T. A Synthetic Model of the Mn_3Ca Subsite of the Oxygen-Evolving Complex in Photosystem II. *Science* **2011**, *333* (6043), 733−736.
(55) Tsui, E. Y.; Agapie, T. Reduction potentials of heterometallic manganese-oxido cubane complexes modulated by redox-inactive metals. *Proc. Natl. Acad. Sci. U. S. A.* **2013**, *110* (25), 10084−10088.
(56) Tsui, E. Y.; Tran, R.; Yano, J.; Agapie, T. Redox-inactive metals modulate the reduction potential in heterometallic manganese−oxido clusters. *Nat. Chem.* **2013**, *5*, 293.
(57) Ray, K.; Pfaff, F. F.; Wang, B.; Nam, W. Status of reactive non-heme metal-oxygen intermediates in chemical and enzymatic reactions. *J. Am. Chem. Soc.* **2014**, *136*, 13942−13958.
(58) Nam, W.; Lee, Y.-M.; Fukuzumi, S. Hydrogen Atom Transfer Reactions of Mononuclear Nonheme Metal−Oxygen Intermediates. *Acc. Chem. Res.* **2018**, *51*, 2014−2022.
(59) Nam, W.; Lee, Y.-M.; Fukuzumi, S. Tuning reactivity and mechanism in oxidation reactions by mononuclear nonheme iron(IV)-oxo complexes. *Acc. Chem. Res.* **2014**, *47*, 1146−1154.
(60) Yin, G.; Danby, A. M.; Kitko, D.; Carter, J. D.; Scheper, W. M.; Busch, D. H. Oxidative Reactivity Difference among the Metal Oxo and Metal Hydroxo Moieties: pH Dependent Hydrogen Abstraction by a Manganese(IV) Complex Having Two Hydroxide Ligands. *J. Am. Chem. Soc.* **2008**, *130* (48), 16245−16253.
(61) Garcia-Bosch, I.; Company, A.; Cady, C. W.; Styring, S.; Browne, W. R.; Ribas, X.; Costas, M. Evidence for a Precursor Complex in C-H Hydrogen Atom Transfer Reactions Mediated by a Manganese(IV) Oxo Complex. *Angew. Chem., Int. Ed.* **2011**, *50* (25), 5648−5653.
(62) Steen, J. D.; Stepanovic, S.; Parvizian, M.; de Boer, J. W.; Hage, R.; Chen, J.; Swart, M.; Gruden, M.; Browne, W. R. Lewis versus Brønsted Acid Activation of a Mn(IV) Catalyst for Alkene Oxidation. *Inorg. Chem.* **2019**, *58*, 14924−14930.

https://dx.doi.org/10.1021/acs.inorgchem.9b02980
Inorg. Chem. 2020, 59, 2689−2700